Author Manuscript

Author Manuscript

Author Manuscript

Author Manuscript

HHS Public Access

Author manuscript

Lab Chip. Author manuscript; available in PMC 2017 October 18.

Published in final edited form as:

Lab Chip. 2016 October 18; 16(21): 4097–4105. doi:10.1039/c6lc00380j.

Bioprinted Thrombosis-on-a-Chip

Yu Shrike Zhang[a,b,c,§], **Farideh Davoudi**[a,b,§], **Philipp Walch**[a,b,d,§], **Amir Manbachi**[a,b,§], **Xuan Luo**[a,b,e,†], **Valeria Dell'Erba**[a,b,f,†], **Amir K. Miri**[a,b], **Hassan Albadawi**[g], **Andrea Arneri**[a,b], **Xiaoyun Li**[a,b,h], **Xiaoying Wang**[a,b,h], **Mehmet Remzi Dokmeci**[a,b,c], **Ali Khademhosseini**[a,b,c,i,j,*], and **Rahmi Oklu**[a,b,k,*]

[a]Biomaterials Innovation Research Center, Division of Biomedical Engineering, Department of Medicine, Brigham and Women's Hospital, Harvard Medical School, Cambridge, MA 02139, USA

[b]Harvard-MIT Division of Health Sciences and Technology, Massachusetts Institute of Technology, Cambridge, MA 02139, USA

[c]Wyss Institute for Biologically Inspired Engineering, Harvard University, Boston, MA 02115, USA

[d]Institute of Pharmacy and Molecular Biotechnology, Heidelberg University, Im Neuenheimer Feld 364, D-69120, Germany

[e]Université de Technologie de Compiègne, Rue du Dr Schweitzer, Compiègne 60200, France

[f]Department of Biomedical Engineering, Politecnico di Torino, 10129 Torino, Italy

[g]Department of Surgery, Division of Vascular and Endovascular Surgery, Massachusetts General Hospital, Boston, MA 02114, USA

[h]State Key Laboratory of Pulp and Paper Engineering, South China University of Technology, Guangzhou, 510640, P.R. China

[i]Department of Bioindustrial Technologies, College of Animal Bioscience and Technology, Konkuk University, Hwayang-dong, Gwangjin-gu, Seoul 143-701, Republic of Korea

[j]Department of Physics, King Abdulaziz University, Jeddah 21569, Saudi Arabia

[k]Division of Vascular & Interventional Radiology, Mayo Clinic, Scottsdale, AZ 85259, USA

Abstract

Thrombosis and its complications are among the most prevalent medical problems. Despite advancements in medical therapies, there is often incomplete resolution of these issues. The residual thrombus can undergo fibrotic changes over time through invaded fibroblasts from the surrounding tissues and eventually lead to the formation of a permanent clot. In order to understand the importance of cellular interactions and the impact of potential therapeutics to treat

*Corresponding Authors: oklu.rahmi@mayo.edu; alik@bwh.harvard.edu.
§Y.S.Z., F.D., P.W., A.M. contributed equally as primary authors.
†X.L., V.D. contributed equally as second authors.

Author Contributions

Y.S.Z., R.O., and A.K. conceived the original concept, supervised the project, and revised the manuscript. Y.S.Z. designed and performed the experiments, and analyzed the data; F.D., P.W., X.L., V.D., A.K.M., H.A., A.A. performed the experiments and analyzed the data; M.R.D. provided technical guidance and revised the manuscript; X.Y.L. and X.Y.W. participated in the revision of the work.

Author Manuscript Author Manuscript Author Manuscript Author Manuscript

thrombosis, an *in vitro* platform using human cells and blood components would be beneficial. Towards achieving this aim, there have been studies utilizing the capabilities of microdevices to study the hemodynamics associated with thrombosis. In this work, we have further exploited the utilization of 3D bioprinting technology, for the construction of a highly biomimetic thrombosis-on-a-chip model. The model consisted of microchannels coated with a layer of confluent human endothelium embedded in a gelatin methacryloyl (GelMA) hydrogel, where human whole blood was infused and induced to form thrombi. Continuous perfusion with tissue plasmin activator led to dissolution of non-fibrotic clots, revealing clinical relevance of the model. Further encapsulating fibroblasts in the GelMA matrix demonstrated the potential migration of these cells into the clot and subsequent deposition of collagen type I over time, facilitating fibrosis remodeling that resembles the *in vivo* scenario. Our study suggests that *in vitro* 3D bioprinted blood coagulation models can be used to study the pathology of fibrosis, and particularly, in thrombosis. This versatile platform may be conveniently extended to other vascularized fibrosis models.

Introduction

Thrombosis and its complications are among the principal reasons for morbidity and mortality caused by cardiovascular diseases.[1–4] Thrombosis can occur in both veins and arteries. Venous thromboembolism includes deep-vein thrombosis and pulmonary embolism.[4] While hemostasis is a physiological response to the vascular injury and is locally limited to the site of bleeding, thrombotic events are the pathologic response to this type of injury, and can lead to partial or complete obstruction of vessel lumen and impairment of the blood flow.[5, 6] The endothelium plays a key role in normal vessel homeostasis through secretion of prostaglandins and nitric oxide, as well as expression of thrombomodulin and antithrombin binding sites, which together contribute to an anticoagulant state.[5, 7, 8] Endothelial injury leads to the activation of the coagulation cascade (secondary hemostasis) that occurs simultaneously with the primary hemostasis.[5, 7, 8] During primary hemostasis, a platelet plug is immediately formed to stop the initial bleeding (Fig. 1A). First, platelets adhere to the von Willebrand factor (vWF) in the endothelial layer. Platelet adhesion results in platelet activation and degranulation; subsequently, platelets aggregate through integrin, which binds platelets to fibrinogen.[8] The secondary hemostasis relies on activation of plasma clotting factors, leading to fibrin formation from its fibrinogen precursor. Fibrin crosslinking by plasma factor XIII stabilizes the thrombus formed during the primary hemostasis process.[5, 7–9]

An acute thrombotic event may require administration of thrombolytic agents, such as tissue plasminogen activator (tPA), as therapy. This agent converts plasminogen to plasmin, which degrades fibrin (fibrinolysis) (Fig. 1B).[10–13] However, there is often incomplete resolution of the thrombus; infiltration and proliferation of pericytes, including fibroblasts and smooth muscle cells, into the thrombus from the surrounding tissue can lead to thrombus fibrosis and organization (Fig. 1C).[14–19] This cellular activity remodels the thrombus into a connective fibers-rich thrombus, mainly comprised of collagen type I (Fig. 1C).[15, 16, 20–22] This remodeling process further reduces the physiologic breakdown of the thrombus and the overall efficacy of anticoagulation/thrombolytic therapy (Fig. 1B).[10, 23–28] The resulting venous wall stiffness and venous hypertension,[20, 29] may clinically manifest as post-

Author Manuscript Author Manuscript Author Manuscript Author Manuscript

thrombotic syndrome, causing edema, pain, and in severe cases ulceration of the affected limb.[14, 17]

In order to understand the importance of cellular interactions and the impact of potential therapeutics to treat thrombosis, the use of an *in vitro* biomimetic platform derived from human cells and blood components would be highly beneficial. So far, several microdevices have been reported to investigate the hemodynamics associated with thrombosis or to mimic the vascular microenvironments.[30–36] In a recent work, thrombosis was modeled in a microfluidic device using disturbed flow.[31] The recirculating flow distal to a stenosis initiated coagulation and therefore led to thrombus formation. In another example, a lithographic method was used to create a microvascular network embedded in a collagen hydrogel, which was further endothelialized and spiked to alter the phenotype of endothelial cells to pro-thrombotic.[30] However, these approaches are limited in their ability to mimic the various structural and biological aspects of blood vessels and utilize relatively complex fabrication procedures.

In contrast, 3D bioprinting of biomaterials and cells in a spatially controlled manner has emerged as an enabling and versatile technology to produce complex tissue constructs including the vasculature.[37–41] Here, we have adapted the use of a 3D sacrificial bioprinting technique,[38] to generate a highly biomimetic human thrombosis-on-a-chip model. The model consisted of hollow microchannels coated with a confluent layer of endothelium embedded in a gelatin methacryloyl (GelMA) hydrogel (Fig. 1D). Human whole blood was infused into the microchannels immediately following thrombosis activation. Subsequently, dynamic studies were performed under flow within bifurcated thrombosed microchannels. Continuous perfusion with tPA was used to assess the dissolution of the non-fibrotic clots and demonstrate the clinical relevance of the model. The hydrogel microchannels encapsulating fibroblasts were further fabricated to simulate fibrosis and aging resembling the *in vivo* scenario and study the deposition of collagen type I in the clot over time.

Experimental section

Cell culture

Human umbilical vein endothelial cells (HUVECs) expressing green fluorescent protein (GFP) (Angio-Proteomie) were cultured in endothelial growth medium (EGM, Lonza). Human dermal fibroblasts (CRL-2522, ATCC) were maintained in Dulbecco's Modified Eagle's Medium (DMEM, ThermoFisher) supplemented with 10 vol.% fetal bovine serum (FBS, ThermoFisher) and 1 vol.% penicillin-streptomycin (ThermoFisher).

GelMA synthesis

GelMA was prepared according to our established protocol.[42] Briefly, gelatin from porcine skin (Sigma-Aldrich) was dissolved in Dulbecco's phosphate buffer saline (DPBS, ThermoFisher) for 2 h at 60 °C under constant stirring to yield a 10 wt.% gelatin solution. To modify with methacryloyl groups, a volume corresponding to 4 vol.% of the gelatin mixture of methacrylic anhydride (Sigma-Aldrich) was added gradually to the gelatin solution and subsequently incubated and stirred for 1 h at 60 °C and 500 rpm. Two volumes

Author Manuscript Author Manuscript Author Manuscript Author Manuscript

of pre-heated DPBS were then added and the solution was dialyzed for at least 5 days. After dialysis, GelMA solution was filtered and freeze-dried.

Sacrificial bioprinting

We fabricated three different types of hydrogel microchannels using the sacrificial bioprinting approach: *i*) microchannels covered by HUVECs without fibroblasts (control), *ii*) non-endothelialized microchannels with encapsulated fibroblasts in the hydrogel, and *iii*) endothelialized microchannels with simultaneously encapsulated fibroblasts inside the matrix (Fig. 1D). To create microchannels, 5 wt.% GelMA in FBS was mixed with 0.2 wt.% 2-hydroxy-4′-(2-hydroxyethoxy)-2-methylpropiophenone (photoinitiator, PI, Sigma-Aldrich). For samples containing fibroblasts, the cells were resuspended in this GelMA solution at a final concentration of 3×10^6 cells mL^{-1}. Using a bioprinter (BioBots, Inc.) equipped with a 27G blunt needle , a 3D sacrificial scaffold made of 40 wt.% Pluronic F-127 (Sigma-Aldrich) in water was generated according to a computer-aided design (CAD) model (Fig. 2A i and Supplementary Video S1). Following overnight dehydration (Fig. 2A ii), the printout was placed on top of a polydimethylsiloxane (PDMS, Sylgard 184 Elastomer Kit, Dow Corning, weight ratio monomer to crosslinking agent 10:1) mold of 8 mm (length) × 4 mm (width) × 4 mm (height) in size (Fig. 2A iii), filled with GelMA prepolymer, and cured from both sides under UV (power: 850 mW, OmniCure Series 2000) (Fig. 2A iv). After crosslinking of GelMA, the block was placed in cold DPBS and left at 4 °C for 15 min (Fig. 2A v). The liquefied sacrificial scaffold of Pluronic F-127 was then removed using a syringe (Fig. 2A vi). For the blocks that contained an endothelial layer, HUVECs were seeded in the channels at a density of 12×10^6 cells mL^{-1}, and left for 30 min on each side. The cell-laden blocks were then placed back inside a tissue culture incubator set at 37 °C for subsequent culture.

Measurement of mechanical properties

Compressive tests were performed to evaluate the mechanical properties of the hydrogel matrix. Specifically, rectangular molds were filled by GelMA pre-polymer and then exposed to UV light for 10 s, 15 s, 20 s, and 25 s. Afterwards the samples were retrieved from the molds and allowed to swell for 6 h in DPBS and reach equilibrium. The samples were places on the lower plate of an Instron mechanical tester, compressed with a 10-N load cell at a strain rate of 0.2 mm min^{-1} by the upper plate. Measurements were carried out at room temperature. Compressive moduli of the hydrogels were derived from the regression of the linear region of stress-strain curves (10–20% strain). The burst pressure was also measured for a set of non-cellular blocks. Using Instron tester in compression testing configuration, a 100-N load cell was attached to a 10-mL syringe filled with DPBS connected to the channel in a block. An estimation of the flow pressure (under a quasi-static 0.01 mL s^{-1} rate) was calculated by comparing loading and unloading histories. The load at which the gel burst was recorded as burst pressure.

Blood infusion

Citrated human whole blood was purchased from Research Blood Components. To induce clotting, 10 vol.% of 0.1 M $CaCl_2$ (Sigma-Aldrich) aqueous solution was added to the blood and the mixture was immediately injected to the microchannels using a 30G syringe needle.

Author Manuscript Author Manuscript Author Manuscript Author Manuscript

After stabilizing the clots for at least 10 min, the samples were gently washed with pre-warmed DPBS and transferred back to media.

Cell viability and morphology analyses

To measure cell viability, the samples were stained with a live/dead kit (ThermoFisher) for 15 min at 37 °C. Cell morphology was assessed *via* f-actin/nuclei staining. After fixation with 4% paraformaldehyde (Electron Microscopy Sciences), f-actin and nuclei staining was performed using Alexa 594-phalloidin (ThermoFisher) and 4′,6-diamidino-2-phenylindole (DAPI, ThermoFisher), respectively, according to manufacturer's instructions. Images were taken using a fluorescence microscope (Zeiss Axio Observer D1). At least five images were taken per sample and analyzed using ImageJ.

Immunostaining and histology

For immunostaining, CD31 antibody (mouse anti-human from Dako, M0823, 1:40) and collagen I antibody (rabbit anti-human from Abcam, ab34710, 1:100) were used. Samples were fixed in 4% paraformaldehyde for overnight at 4 °C. Primary antibodies were allowed to incubate with the samples for overnight at 4 °C. Secondary antibodies (goat anti-rabbit, labeled with Alexa Fluor 647, and rabbit anti-mouse, labeled with Alexa Fluor 488; ThermoFisher) were subsequently added and incubated at room temperature for 1 h. Nuclei were counterstained with DAPI. To assess thrombus morphology inside the microchannels the samples were subjected to standard fixation and paraffin sectioning procedure (10-μm thickness) followed by staining with hematoxylin/eosin. Images were taken using a fluorescence microscope.

Perfusion assay

For the perfusion assay, a bifurcation geometry was adopted. The bifurcation configuration was chosen to allow tPA to continuously flow through the open arm while diffusing into the other thrombosed arm to dissolve the clot, simulating the *in vivo* scenario. In the case of a straight channel, the introduction of a blood clot would lead to complete blockage of the channel and therefore prohibit perfusion studies.

To study the flow dynamics, DPBS containing suspended fluorescent microbeads (Createx Colors, East Granby) was perfused from the inlet and the flow movements were recorded using a fluorescence microscope (Zeiss). An ImageJ plug-in JPIV,[43] was used to analysis the fluid velocity at three regions: inlet, bifurcation point, and the outlet.

Prior to perfusion, a thrombus was introduced to the longer arm of the bifurcated microchannels as described above. Perfusion was performed on samples at days 1 and 7 after clotting using a syringe pump (New Era Pump Systems) equipped with 3-mL syringes connected to the samples *via* Tygon tubing (Cole Parmer) and metal connectors (Instech). As instructed by the manufacturer (Alteplase, Genentech), tPA was reconstituted with buffer at a concentration of 1 mg mL^{-1}. Perfusion with tPA was performed at a flow rate of 1 mL h^{-1} for up to 2 h. This flow rate was chosen to resemble the physiological conditions present in human venous blood vessels in the legs where thrombosis are commonly formed.[44–46]

Author Manuscript Author Manuscript Author Manuscript Author Manuscript

Results and discussions

Sacrificial 3D bioprinting of vascularized constructs

Sacrificial bioprinting has proved its utility in fabricating hydrogel constructs containing hollow microchannels mimicking the vasculature.[37–40] We first deposited a mold consisting of a sacrificial scaffold using Pluronic and allowed it to dry overnight. We subsequently filled the mold with GelMA solution and induced gelation using photocrosslinking. Afterwards, the Pluronic structures were removed by immersing the entire construct in a cold PBS to achieve a hydrogel microchannel (Fig. 2A and B). Compared to the previously reported methods,[37–40] our approach provides improved control over the molding process by integrating not only the microchannel structures but also the frame to hold the hydrogel in place during fabrication. The resolution of the printed channels is controlled by the needle size and the speed at which the nozzle is moved. The geometry is dependent on the path of the nozzle movement. Accordingly we have fabricated GelMA constructs containing a series of microchannel diameters and tortuosity to indicate our capability to model blood vessels of various properties (Supplementary Fig. S1). It should be further noted that, the shear-thinning behavior of the 40% Pluronic aqueous solution ensured that the extruded bioink could immediately return to its gel state and retain the cylindrical shape to allow for construction of circular channels within the GelMA block.[39]

To mimic the endothelium, GFP-expressing HUVECs were seeded into the microchannels and cultured until confluency was reached. Fig. 2Ci shows the HUVECs covering the interior surface of a linear microchannel immediately after fabrication and at 1 and 2 days post-seeding. The spreading of HUVECs on the inner surface of the microchannel started shortly after seeding to form a confluent endothelium lining along the length of the microchannel by day 2. For the bifurcating channels similar trends were observed along the entire microchannels, including the point of bifurcation (Fig. 2C ii). This is crucial as the generation of comparable dynamic flows within the two arms of the channels is mainly dependent on the homogenous properties of the channels and the coated endothelial cells at the junction point. Immunostaining for CD31 and nuclei further confirmed the functionality of the endothelium covering the microchannel walls (Fig. 2C iii).

Thrombus formation and thrombolysis

We subsequently explored the potential application of the vascularized hydrogel microchannels as a model for studying thrombosis. In order to induce thrombosis, 10 vol.% 0.1-M $CaCl_2$ in DPBS was added to pooled human whole blood and immediately injected into the microchannels in the hydrogels. The capillary force induced spontaneous filling of the microchannels by the blood (Fig. 3A i), where clotting was observed to occur within approximately 10 min (Fig. 3A ii). The clots were subsequently allowed to stabilize for another 20 min before returning the samples to the culture medium for further observation of clot maturation and transformation. Representative micrographs of the thrombus formed in a microchannel are shown in Fig. 3B. Red blood cells (RBCs) aggregating in the microchannel were clearly observed. In addition, the thrombosed microchannels were subjected to histology analysis, where transverse paraffin sections were obtained and stained using H&E (Fig. 3C i and ii). As expected, thrombi successfully formed in both the plain

Author Manuscript Author Manuscript Author Manuscript Author Manuscript

microchannel as well as endothelialized microchannel, filling the entire volume of the lumen. For the thrombosis-on-chip model formed with endothelium, a monolayer of endothelial cells was present on the surface of the microchannel, functioning as a barrier that separated the surrounding matrix with the clot, closely mimicking the *in vivo* scenario. H&E staining of a venous thrombus *in vivo* from a patient sample is shown in Fig. 3C iii, where no migration of pericytes was observed in the presence of an intact layer of endothelium.

It is important for the thrombosis-on-chip model to recapitulate the *in vivo* thrombolytic activities of the clots upon treatment with thrombolytic agents. Physiologically, administration of thrombolytic agents such as tPA to a non-fibrotic clot would result in thrombolysis (Fig. 1B).[10–13] Therefore, we adopted the bifurcation microchannel configuration to verify the thrombolytic potential of tPA in our thrombosis-on-a-chip model (Fig. 3D). The bifurcation configuration was chosen to allow tPA to continuously flow through the open arm while diffusing into the other thrombosed arm to dissolve the clot, simulating the *in vivo* scenario. On the contrary, in the case of a straight channel the introduction of a blood clot would lead to complete blockage of the channel and therefore prohibit perfusion studies.

To study the flow dynamics in the bifurcation setup, the end of the longer arm of the bifurcation was sealed by removing the corresponding sacrificial segment prior to the GelMA casting process. Particle image velocimetry (PIV) was used to quantitatively analyze the flow velocity profiles (Supplementary Movie S2).[47] The mean velocities were used to estimate the Reynold numbers, in which they were consistently lower than 0.5 for flow rates between 0.6 and 3 mL h^{-1}. This result confirmed the presence of laminar flow in the bifurcation channel within the chosen range of perfusion flow rate. The mean velocities along the main channel fell between 0.19 ± 0.06 mm s^{-1} and 0.54 ± 0.16 mm s^{-1} for the flow rate range applied, similar to those found in human blood vessels in the legs where thrombosis are commonly formed.[44–46] An intermediate flow rate of 1 mL h^{-1} was then selected for the subsequent thrombolysis studies. The burst pressure of the microchannel-containing GelMA construct (5 wt.%, 15-s crosslinking) was measured to be 0.16 ± 0.08 kPa, sufficient to withstand the pressure caused by such a flow rate.

After confirming the laminar flow profile of the bioprinted bifurcation configuration at the selected perfusion flow rate, thrombolysis experiments were subsequently performed. Thrombosis was selectively formed in the longer arm of the bifurcation, where clinically relevant concentration of tPA (1 mg mL^{-1}) was slowly perfused from the common inlet at the flow rate of 1 mL h^{-1} for up to 2 h, allowing for continuous exposure of the thrombus with tPA during the perfusion period while minimizing its potential physical dislocation caused by fluid pressure. Using this setup, we observed the dissolution of the clots in the microchannels with tPA treatment for non-fibrotic thrombi formed after both 1 day (Fig. 3E i) and 7 days (Fig. 3E ii). To our knowledge *in vitro* investigation of thrombolytic events have not been realized before with conventional microfabrication approaches. This result clearly illustrated the biomimetic properties of our *in vitro* bifurcation thrombosis model fabricated using sacrificial bioprinting and its potential future use in systematic study of thrombosis, thrombolysis, and related pathologies. However, it is noteworthy to point out that in the current investigation quantification of the thrombolytic events has not been

Author Manuscript Author Manuscript Author Manuscript Author Manuscript

achieved, due to the challenges associated with mechanical instability when handling the hydrogel constructs that would lead to physical dislodge of the thrombi and thus the inability to quantitatively assess the remaining clots within the microchannels. We believe that future applications of this thrombosis model will benefit from additional studies involving quantification of the thrombolysis process potentially in conjunction with their comparisons with patient data.

Co-culture with fibroblasts

Once formed, the thrombus can further undergo fibrotic changes due to the invasion of fibroblasts into the clot from the surrounding tissue *via* the damaged endothelium.[14–19] Overtime, this cellular activity leads to remodeling by transforming a thrombus into a connective tissue-rich clot, mainly comprised of collagen type I (Fig. 1C),[15, 16, 20–22] further preventing the breakdown of the thrombus (Fig. 1B).[10, 23–25] To better recapitulate such biological process *in vitro*, we subsequently introduced fibroblasts into our hydrogel matrix for co-culture with the endothelial cells to model the vascular microenvironment in the human body.

Fibroblast-containing hydrogel microchannels were formed by mixing cells with the pre-polymer solution and then molding the mixture onto the bioprinted sacrificial template. The resulting mixture was then photocrosslinked. Fig. 4A and B depict the influence of UV exposure duration on the viability of the encapsulated fibroblasts. The viability of fibroblasts decreased over the culture period and with increasing UV light exposure. Fibroblasts maintained high viability in hydrogel matrices for UV exposures of 10 s and 15 s, at >80% for up to 7 days analyzed. In comparison, a significant decrease in viability of fibroblasts at later stages was observed for constructs that were crosslinked for 20 s and 25 s, likely due to the adverse effects caused by UV light illumination. This result is consistent with our previous observations on the effect of UV exposure on cell viability, where longer exposure times caused increased death of cells embedded in GelMA hydrogels.[48]

Mechanical properties of the hydrogel matrix have also been shown to affect the spreading and migration of encapsulated cells.[42] To determine the effect of UV light exposure on the modulus of the matrix, unconfined compression was performed for blocks undergone 10 s, 15 s, 20 s, and 25 s of light crosslinking (Fig. 4C). We observed the highest average modulus of approximately 0.8 kPa for a crosslinking time of 25 s and the lowest of around 0.65 kPa for 10-s irradiation; the 15-s and 20-s light exposures resulted in moduli of approximately 0.7 kPa and 0.75 kPa, respectively. However, no significant differences were observed among the samples undergone various crosslinking densities for our current formulation of 5 wt.% GelMA and 0.2 wt.% PI. These results are consistent with those reported in literature for GelMA hydrogels fabricated under similar conditions, where mechanical properties within this range (0.5–1 kPa) have been shown to support the growth of fibroblasts.[42] Since spreading of the fibroblasts is crucial for successful encapsulation and subsequent migration, f-actin staining was further performed. Fig. 4D shows the morphology of the fibroblasts encapsulated inside GelMA hydrogels (10 s and 15 s crosslinking) after 7 days of culture, clearly indicating their spreading in the matrix. For prolonged UV crosslinking times of 20 s

Author Manuscript Author Manuscript Author Manuscript Author Manuscript

and 25 s, the spreading of the encapsulated fibroblasts was limited, likely due to the significantly reduced viability of the cells especially at later stages of culture (Fig. 4A).

Based on these results we used a photocrosslinking time of 15 s for the construction of vascularized hydrogel microchannels encapsulating fibroblasts, due to the excellent cell spreading and relatively high cell viability (>80%) across the entire culture period. It was found that the co-culture of HUVECs seeded inside the microchannel and fibroblasts within the GelMA hydrogel did not affect the behaviors of the cells. By day 3 a confluent layer of endothelium could be formed to cover the entire inner surface of the microchannel while the fibroblasts were observed to proliferate and spread in the matrix (Fig. 4E). These results demonstrated our ability to generate vascularized microchannels encapsulating fibroblasts in the hydrogel using the sacrificial bioprinting technique, in an effort to mimic the *in vivo* microenvironment.

Formation of fibrotic clots

We anticipated that the encapsulation of fibroblasts in the matrix of hydrogel microchannels would form a more *in vivo*-like microenvironment and facilitate fibrosis of the thrombus through migration of fibroblasts into the vascular lumen when the integrity of the endothelium is compromised (Fig. 1C). To test this hypothesis, we fabricated three types of models (Fig. 1D): *i*) endothelialized microchannel without fibroblasts in the hydrogel as the control; *ii*) non-endothelialized microchannel with fibroblasts in the matrix to mimic the damaged vessel; and *iii*) endothelialized microchannel with fibroblasts in the matrix to mimic the normal vessel. It was expected that in the model with damaged vessel the fibroblasts would migrate into the clot and/or proliferate at the interface of the microchannel and the clot to deposit collagen matrix, whereas no fibrosis and collagen secretion should be observed in the vicinity of the clot in the model with intact endothelium, mimicking the *in vivo* scenario (Fig. 5A and Fig. 3C iii). To test this hypothesis, thrombosis was induced to form in all three types of models following the procedure mentioned previously. The thrombosis-on-chip models were continued in culture for up to 14 days and then immunostained for CD31 and collagen type I.

Fig. 5B shows the results from immunostaining for the three types of thrombosis models. In the model containing an intact endothelial layer on the surface of the microchannel but without encapsulated fibroblasts in the hydrogel, no staining for collagen I was visible in the blood clot even by the end of day 14, as expected (Fig. 5b i). The staining for CD31 clearly indicated the confluent endothelium (Fig. 5B i). In contrast, in the model where no HUVECs were present, the fibroblasts exhibited pronounced invasion and/or proliferation in the vicinity of the clot followed by deposition of collagen I inside the thrombus (Fig. 5B ii). Such a model could be considered as a representative scenario of fibrosis where the endothelial layer of the vasculature is partially damaged, facilitating fibroblast migration into the thrombus and subsequent collagen secretion. Finally, in the presence of the endothelium, even when the fibroblasts were encapsulated inside the surrounding matrix, they could not cross the endothelial barrier to reach the thrombus as indicated by the absence of collagen I (Fig. 5B iii), mimicking the scenario during the formation of a venous thrombus *in vivo* where an intact endothelium is present (Fig. 3C iii). It should be noted that

Author Manuscript Author Manuscript Author Manuscript Author Manuscript

the artifacts in the integrity of the endothelium observed in the images were largely caused by the cryosectioning process where the layer was easily detached at the initial site of cutting due to the mismatching mechanical properties/limited adhesion of the cells and the surrounding hydrogel. Quantification data on relative collagen I expression (Fig. 5C) further supported microscopic observations.

The biomimetic human thrombosis-on-a-chip model described in this study provides us with the capability to conduct *in vitro* studies aiming towards resemblance of thrombosis and its variations such as fibrosis, at a level surpassing the existing comparable studies in the literature. In particular, 3D bioprinting in a spatially controlled fashion allowed us to create realistic structures such as bifurcated vasculature. This feature provides us with a unique flexibility in comparison with the device that reported thrombus formation achieved through the introduction of rigid stenosis and hence disturbed flow within a microfluidic chamber.[31] Another importance aspect associated with the thrombosis-on-a-chip platform described in this study lies in our ability to endothelialize the channels from within, in close adjacency to the fibroblast cells embedded within the hydrogel. This co-culture aspect of our platform allows for studying unique aspects of thrombosis, such as migration of fibroblasts, and the ability to study clot aging, thereby facilitating the construction of a fibrotic-clot-on-a-chip model that has not been achieved before.[30] This study is also the first of its kind to the best of our knowledge, demonstrating proof-of-principle dynamic perfusion of blood flow within bifurcated thrombosed microchannels, where tPA was used to assess the dissolution of the non-fibrotic clots.

Conclusions

In this study, we employed a sacrificial 3D bioprinting approach for the fabrication of a proof-of-concept human thrombosis-on-a-chip platform. The model contained hollow microchannels coated with layer of confluent endothelial layers. The microchannels were embedded within GelMA hydrogels with or without encapsulated fibroblasts. Human whole blood was infused into the microchannels to form thrombi and continuous perfusion of tPA as a thrombolytic agent demonstrated potential dissolution of the non-fibrotic clots. It was further observed that, in the hydrogels containing fibroblasts and damaged endothelium, migration of fibroblasts into the clot and deposition of collagen type I occurred, confirming the biomimicry of the model in recapitulating the fibrosis process *in vivo*. Our results indicate that this novel *in vitro* thrombosis-on-a-chip platform can function as a powerful model for studying thrombosis, thrombolysis, and fibrosis as well as the interactions among different components. This versatile platform may be further extended to other vascularized fibrosis models.

Further studies may benefit from better understanding of the thrombosis/thrombolysis events within the bioprinted in hydrogel constructs involving more thorough quantitative analyses. While current study only investigated the effect of invading fibroblasts, smooth muscle cells may also be incorporated into the model in the future due to their unique contributions in cases of vascular injuries.[49, 50] The use of tissue-specific and potentially patient-derived cells would bring the model additional applications gearing towards personalized vascular disease modeling.

Author Manuscript Author Manuscript Author Manuscript Author Manuscript

Supplementary Material

Refer to Web version on PubMed Central for supplementary material.

Acknowledgments

The authors acknowledge funding from the Office of Naval Research Young National Investigator Award, the National Institutes of Health (EB012597, AR057837, DE021468, HL099073, R56AI105024, AR068258, AR066193, EB022403, EB021148), and the Presidential Early Career Award for Scientists and Engineers (PECASE). Y.S.Z. acknowledges the National Cancer Institute of the National Institutes of Health Pathway to Independence Award (1K99CA201603-01A1). R.O. acknowledges additional support from Mayo Clinic.

References

1. Davies MJ, Thomas A. New Engl J Med. 1984; 310:1137–1140. [PubMed: 6709008]
2. Falk E, Fernández-Ortiz A. The American journal of cardiology. 1995; 75:5B–11B.
3. Mai C, Hunt D. The American journal of medicine. 2011; 124:402–407. [PubMed: 21531227]
4. Heit JA, Silverstein MD, Mohr DN, Petterson TM, Lohse CM, O'Fallon WM, Melton LJ III. Thromb Haemost. 2001; 86:452–463. [PubMed: 11487036]
5. Owens AP III, Mackman N. Thrombosis and Haemostasis. 2010; 104:432–439. [PubMed: 20539911]
6. Furie B, Furie BC. New Engl J Med. 2008; 359:938–949. [PubMed: 18753650]
7. Breitenstein A, Tanner FC, Luscher TF. Circ J. 2010; 74:3–12. [PubMed: 19996531]
8. Versteeg HH, Heemskerk JWM, Levi M, Reitsma PH. Physiol Rev. 2013; 93:327–358. [PubMed: 23303912]
9. Oklu R, Albadawi H, Watkins MT, Monestier M, Sillesen M, Wicky S. J Vasc Interv Radiol. 2012; 23:712–718. [PubMed: 22525027]
10. Jaff MR, McMurtry MS, Archer SL, Cushman M, Goldenberg N, Goldhaber SZ, Jenkins JS, Kline JA, Michaels AD, Thistlethwaite P, Vedantham S, White RJ, Zierler BK. C. Amer Heart Assoc Council, D. Council Peripheral Vasc and T. Council Arteriosclerosis. Circulation. 2011; 123:1788–1830. [PubMed: 21422387]
11. Kunadian V, Gibson CM. Cardiovasc Ther. 2012; 30:e81–e88. [PubMed: 21070617]
12. O'Gara PT, Kushner FG, Ascheim DD, Casey DE, Chung MK, de Lemos JA, Ettinger SM, Fang JC, Fesmire FM, Franklin BA, Granger CB, Krumholz HM, Linderbaum JA, Morrow DA, Newby LK, Ornato JP, Ou N, Radford MJ, Tamis-Holland JE, Tommaso CL, Tracy CM, Woo YJ, Zhao DX. J Am Coll Cardiol. 2013; 61:E78–E140. [PubMed: 23256914]
13. Wardlaw JM, Murray V, Berge E, del Zoppo G, Sandercock P, Lindley RL, Cohen G. Lancet. 2012; 379:2364–2372. [PubMed: 22632907]
14. Deatrick KB, Eliason JL, Lynch EM, Moore AJ, Dewyer NA, Varma MR, Pearce CG, Upchurch GR, Wakefield TW, Henke PK. Journal of Vascular Surgery. 2005; 42:140–148. [PubMed: 16012463]
15. Fineschi V, Turillazzi E, Neri M, Pomara C, Riezzo I. Forensic Science International. 2009; 186:22–28. [PubMed: 19203853]
16. Hara T, Truelove J, Tawakol A, Wojtkiewicz GR, Hucker WJ, MacNabb MH, Brownell AL, Jokivarsi K, Kessinger CW, Jaff MR, Henke PK, Weissleder R, Jaffer FA. Circulation. 2014; 130:1044. [PubMed: 25070665]
17. Nosaka M, Ishida Y, Kimura A, Kondo T. Int J Legal Med. 2009; 123:235–240. [PubMed: 19194719]
18. Saha P, Humphries J, Modarai B, Mattock K, Waltham M, Evans CE, Ahmad A, Patel AS, Premaratne S, Lyons OTA, Smith A. Arterioscler Thromb Vasc Biol. 2011; 31:506–512. [PubMed: 21325673]
19. Wakefield TW, Myers DD, Henke PK. Arterioscler Thromb Vasc Biol. 2008; 28:387–391. [PubMed: 18296594]

Author Manuscript Author Manuscript Author Manuscript Author Manuscript

20. Henke PK, Comerota AJ. Journal of Vascular Surgery. 2011; 53:500–509. [PubMed: 21129900]
21. Nosaka M, Ishida Y, Kimura A, Kondo T. Forensic Science International. 2010; 195:143–147. [PubMed: 20060249]
22. Phinikaridou A, Andia ME, Saha P, Modarai B, Smith A, Botnar RM. Circ-Cardiovasc Imaging. 2013; 6:433. [PubMed: 23564561]
23. Oklu R, Wicky S. Semin Thromb Hemost. 2013; 39:446–451. [PubMed: 23483455]
24. Vedantham S. Am J Hematol. 2012; 87:S113–S118. [PubMed: 22389183]
25. Vedantham S, Millward SF, Cardella JF, Hofmann LV, Razavi MK, Grassi CJ, Sacks D, Kinney TB. J Vasc Interv Radiol. 2009; 20:S332–S335. [PubMed: 19560020]
26. Oklu, R.; Wicky, S. Catheter-directed thrombolysis of deep venous thrombosis. 2013.
27. Ganguli S, Kalva S, Oklu R, Walker TG, Datta N, Grabowski EF, Wicky S. Cardiovasc Intervent Radiol. 2012; 35:1053–1058. [PubMed: 21847709]
28. Wicky, S.; Pinto, EG.; Oklu, R. Catheter-directed thrombolysis of arterial thrombosis. 2013.
29. Kahn SR, Comerota AJ, Cushman M, Evans NS, Ginsberg JS, Goldenberg NA, Gupta DK, Prandoni P, Vedantham S, Walsh ME, Weitz JI. C Amer Heart Assoc, C. Council Clinical and N. Council Cardiovasc Stroke. Circulation. 2014; 130:1636–1661. [PubMed: 25246013]
30. Zheng Y, Chen JM, Craven M, Choi NW, Totorica S, Diaz-Santana A, Kermani P, Hempstead B, Fischbach-Teschl C, Lopez JA, Stroock AD. Proc Natl Acad Sci U S A. 2012; 109:9342–9347. [PubMed: 22645376]
31. Jain A, Graveline A, Waterhouse A, Vernet A, Flaumenhaft R, Ingber DE. Nat Commun. 2016:7.
32. Ting L, Feghhi S, Karchin A, Tooley W, White NJ. Blood. 2013; 122:2363–2363.
33. Colace TV, Tormoen GW, McCarty OJT, Diamond SL. Annu Rev Biomed Eng. 2013; 15:283. [PubMed: 23642241]
34. Li M, Ku DN, Forest CR. Lab Chip. 2012; 12:1355–1362. [PubMed: 22358184]
35. Muthard RW, Diamond SL. Lab Chip. 2013; 13:1883–1891. [PubMed: 23549358]
36. Tsai M, Kita A, Leach J, Rounsevell R, Huang JN, Moake J, Ware RE, Fletcher DA, Lam WA. The Journal of clinical investigation. 2012; 122:408–418. [PubMed: 22156199]
37. Miller JS, Stevens KR, Yang MT, Baker BM, Nguyen DHT, Cohen DM, Toro E, Chen AA, Galie PA, Yu X. Nat Mater. 2012; 11:768–774. [PubMed: 22751181]
38. Bertassoni LE, Cecconi M, Manoharan V, Nikkhah M, Hjortnaes J, Cristino AL, Barabaschi G, Demarchi D, Dokmeci MR, Yang Y. Lab Chip. 2014; 14:2202–2211. [PubMed: 24860845]
39. Kolesky DB, Truby RL, Gladman AS, Busbee TA, Homan KA, Lewis JA. Adv Mater. 2014; 26:3124–3130. [PubMed: 24550124]
40. Lee VK, Kim DY, Ngo H, Lee Y, Seo L, Yoo SS, Vincent PA, Dai G. Biomaterials. 2014; 35:8092–8102. [PubMed: 24965886]
41. Murphy SV, Atala A. Nat Biotechnol. 2014; 32:773–785. [PubMed: 25093879]
42. Nichol JW, Koshy ST, Bae H, Hwang CM, Yamanlar S, Khademhosseini A. Biomaterials. 2010; 31:5536–5544. [PubMed: 20417964]
43. http://www.jpiv.vennemann-online.de/.
44. Kouka, N.; Nass, L.; Feist, W. Compression Therapy Concepts. Femoral Vein Blood Flow Velocities.
45. Fronek A, Criqui MH, Denenberg J, Langer RD. J Vasc Surg. 2001; 33:1050–1056. [PubMed: 11331848]
46. Abraham P, Leftheriotis G, Desvaux B, Saumet M, Saumet JL. Clin Physiol. 1994; 14:15–21. [PubMed: 8149706]
47. Amiri S, Taher R, Mongeau LG. Int J Heat Mass Transfer. 2014; 69:464–472.
48. Colosi C, Shin SR, Manoharan V, Massa S, Constantini M, Barbetta A, Dokmeci MR, Dentini M, Khademhosseini A. Adv Mater. 2015; 28:677–684. [PubMed: 26606883]
49. Ip JH, Fuster V, Badimon L, Badimon J, Taubman MB, Chesebro JH. J Am Coll Cardiol. 1990; 15:1667–1687. [PubMed: 2188991]
50. Schwartz SM, Campbell GR, Campbell JH. Circul Res. 1986; 58:427–444.

Author Manuscript Author Manuscript Author Manuscript Author Manuscript

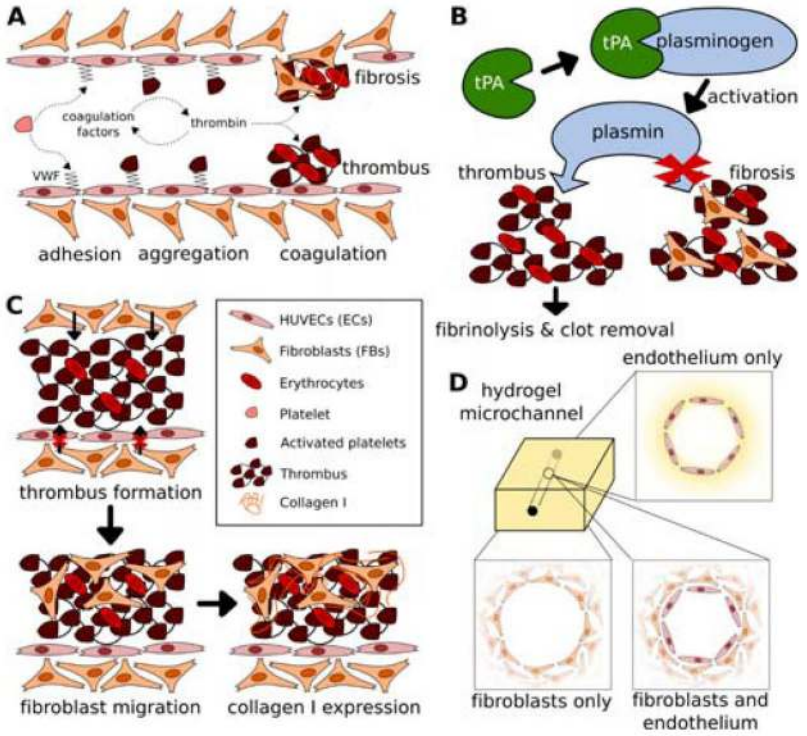

Fig. 1.

Thrombosis, thrombolysis, and biomimetic thrombosis-on-a-chip models. A) Mechanism of thrombus formation and development. After the endothelium damage, platelets adhere to the endothelial layer via the vWF. This leads to the activation and finally aggregation of platelets. Simultaneously, coagulation cascade results in cleavage of fibrinogen to fibrin through thrombin, to eventually form a thrombus. B) Depiction of the tPA thrombolysis mechanism: tPA binds to plasminogen and cleaves it to the active form plasmin, which dissolves a non-fibrotic blood clot but not a fibrotic clot. C) Formation of fibrotic thrombus through fibroblast migration into the blood clot from the surrounding tissue via the damaged endothelium. Collagen type I is then expressed by the invading fibroblasts, leading to fibrosis. D) To model the different aspects of thrombosis and fibrosis, three different types of models were generated: endothelium covering the microchannel wall with no encapsulated fibroblasts in the matrix (control), encapsulated fibroblasts with no endothelial cells covering the microchannel, and both encapsulated fibroblasts in the matrix and endothelium covering the microchannel.

Author Manuscript Author Manuscript Author Manuscript Author Manuscript

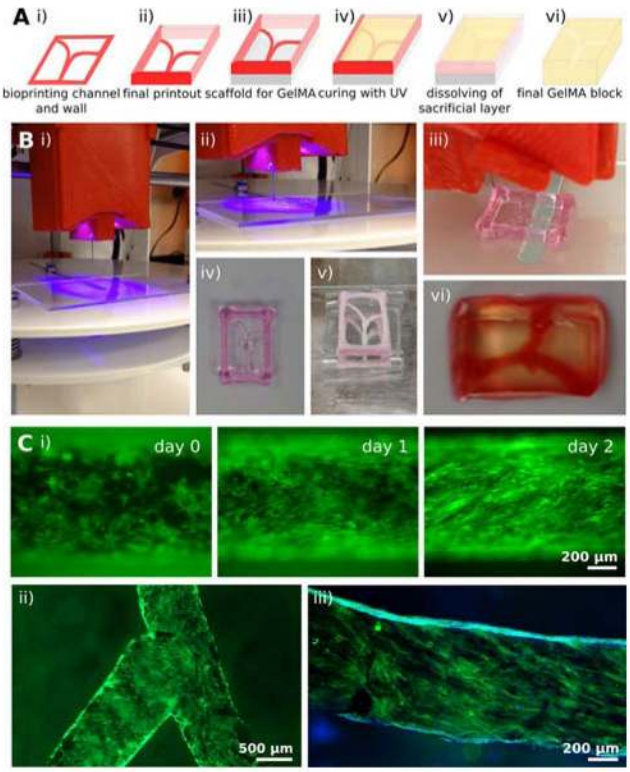

Fig. 2.

Sacrificial bioprinting of vascularized hydrogels. (A) Schematic of the bioprinting process: i, ii) bioprinting of a Pluronic template; iii) dried template is placed on a PDMS support; iv) the mold is filled with GelMA followed by UV crosslinking; v) dissolution of the sacrificial channels and frame to produce vi) the final construct with hollow channels. B) Photographs showing the experimental depiction of the corresponding steps of the sacrificial bioprinting process illustrated in (A). C) Endothelialization of the hollow microchannels inside the GelMA construct for (i) a linear and (ii) bifurcating microchannels; (iii) CD31 (green) and nuclei (blue) staining of the confluent layer of HUVECs.

Author Manuscript Author Manuscript Author Manuscript Author Manuscript

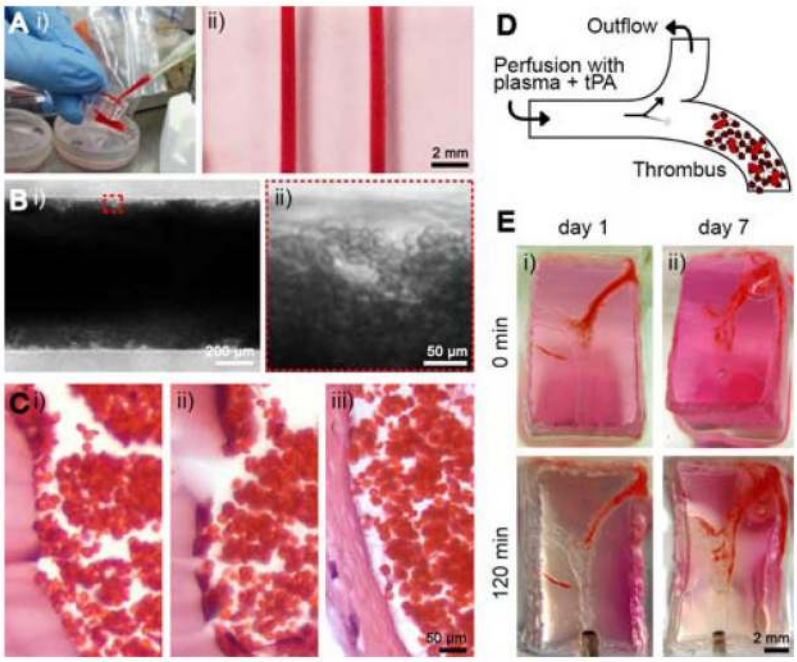

Fig. 3.

Thrombus formation and thrombolysis. (A) Photographs showing (i) the infusion of human whole blood into the endothelialized microchannels and (ii) the formed thrombosis-on-chip model. (B) Optical micrograph showing the formed thrombus in a microchannel, where aggregated red blood cells were clearly observed. (C) Optical micrograph showing H&E-stained transvers sections of (i) a thrombus without HUVECs and (ii) a thrombus with HUVECs, both at 7 days post clotting, and (iii) a venous thrombus formed in vivo at 7 days. (D) Schematic diagram illustrating the tPA thrombolytic study using bifurcated endothelialized microchannels with one branch thrombosed, where tPA is continuously infused to dissolve the clot. (E) Time-lapse photographs showing the thrombolysis of (i) a 1-day clot and (ii) a 7-day clot.

Author Manuscript Author Manuscript Author Manuscript Author Manuscript

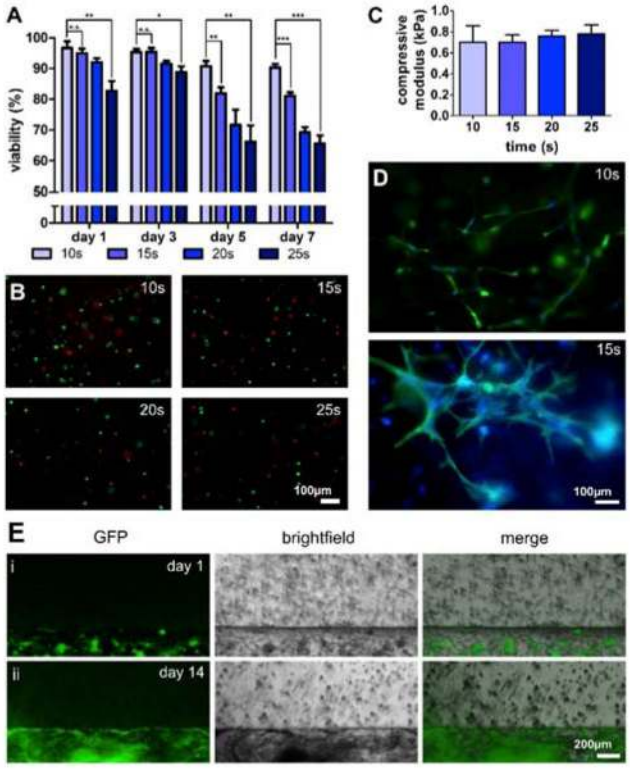

Fig. 4.

Co-culture of fibroblasts with endothelial cells. A) Viability of fibroblasts encapsulated in GelMA hydrogels with various photocrosslinking durations. B) Live/dead analysis of the encapsulated fibroblasts in hydrogels crosslinked under different UV light exposure times at day 1. C) Mechanical properties of GelMA under different light exposure times. D) Spreading of encapsulated fibroblasts at day 7 of culture. E) Micrographs showing co-culture of fibroblasts encapsulated in GelMA hydrogel and HUVECs seeded in the microchannel. (* $p<0.05$, ** $p<0.01$, *** $p<0.001$)

Author Manuscript Author Manuscript Author Manuscript Author Manuscript

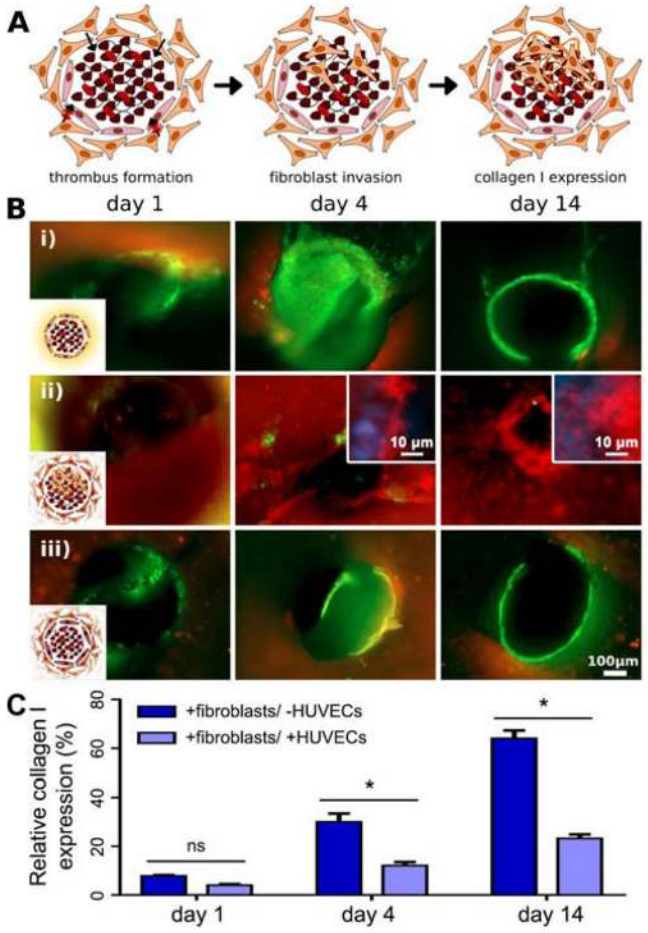

Fig. 5.

Fibrosis of the thrombus. (A) Schematic of the specimens; (B) Immunostaining of different thrombosis-on-chip models, where CD31 (for HUVECs) were stained in green, and collagen type I in red: i) in the presence of HUVECs and absence of fibroblasts, no collagen deposition in the thrombus could be discerned; ii) in the absence of HUVECs and presence of fibroblasts, significant fibrosis of the thrombus occurred; the insets are images counterstained for nuclei indicating the presence of invaded/proliferated fibroblasts; and iii) in the presence of both HUVECs and fibroblasts, no collagen deposition in the thrombus was observed as well due to the endothelial barrier. The artifacts in the integrity of the endothelium observed in the images were mainly caused by the cryosectioning process. (C) Quantification of relative collagen I expression for samples in the presence of fibroblasts with and without HUVECs. ns: not statistically significant; *: $p<0.05$.